The Astrophysical Journal, 782:80 (9pp), 2014 February 20 doi:10.1088/0004-637X/782/2/80

STATISTICAL EQUILIBRIUM OF COPPER IN THE SOLAR ATMOSPHERE

J. R. Shi[1], T. Gehren[2], J. L. Zeng[3], L. Mashonkina[1,4], and G. Zhao[1]
[1] Key Laboratory of Optical Astronomy, National Astronomical Observatories, Chinese Academy of Sciences, Beijing 100012, China; sjr@bao.ac.cn
[2] Universitäts-Sternwarte München, Scheinerstrasse 1, D-81679 München, Germany
[3] Department of Physics, College of Science, National University of Defense Technology, Changsha, Hunan 410073, China
[4] Institute of Astronomy, Russian Academy of Sciences, Pyatnitskaya Str. 48, Moscow 109017, Russia
Received 2013 March 23; accepted 2013 December 23; published 2014 January 30

ABSTRACT

Non-local thermodynamic equilibrium (NLTE) line formation for neutral copper in the one-dimensional solar atmospheres is presented for the atomic model, including 96 terms of Cu I and the ground state of Cu II. The accurate oscillator strengths for all the line transitions in model atom and photoionization cross sections were calculated using the *R*-matrix method in the Russell–Saunders coupling scheme. The main NLTE mechanism for Cu I is the ultraviolet overionization. We find that NLTE leads to systematically depleted total absorption in the Cu I lines and, accordingly, positive abundance corrections. Inelastic collisions with neutral hydrogen atoms produce minor effects on the statistical equilibrium of Cu I in the solar atmosphere. For the solar Cu I lines, the departures from LTE are found to be small, the mean NLTE abundance correction of ∼0.01 dex. It was found that the six low-excitation lines, with excitation energy of the lower level $E_{\rm exc} \leqslant 1.64$ eV, give a 0.14 dex lower mean solar abundance compared to that from the six $E_{\rm exc} > 3.7$ eV lines, when applying experimental gf-values of Kock & Richter. Without the two strong resonance transitions, the solar mean NLTE abundance from 10 lines of Cu I is $\log \varepsilon_{\odot}({\rm Cu}) = 4.19 \pm 0.10$, which is consistent within the error bars with the meteoritic value 4.25 ± 0.05 of Lodders et al. The discrepancy between $E_{\rm exc} = 1.39$–1.64 eV and $E_{\rm exc} > 3.7$ eV lines can be removed when the calculated gf-values are adopted and a mean solar abundance of $\log \varepsilon_{\odot}({\rm Cu}) = 4.24 \pm 0.08$ is derived.

Key words: line: formation – line: profiles – Sun: abundances

1. INTRODUCTION

Understanding the line formation of copper nuclei in cool stars is essential for learning more about nucleosynthesis and stellar masses during Galactic evolution. Copper is primarily an *s*-process nucleus with two stable isotopes. At the lowest metallicities, the manufacture of Cu could be due to several different nucleosynthetic processes (Pignatari et al. 2010). The scientific importance in studying the abundance of Cu is because the astrophysical site for the synthesis of Cu is not yet well established, and the study of [Cu/Fe] in stars of different metallicities gives an important indication of the nucleosynthetic processes derived from the progenitor stars that contribute to the formation of this element (Sneden et al. 1991; Mishenina et al. 2002; Bihain et al. 2004).

Observations of copper abundances rely mostly on the Cu I optical lines, Prochaska et al. (2000) used the strongest line in the near-infrared, while Bihain et al. (2004) and Cohen et al. (2008) used the resonance lines at the UV region. They found that the behavior of [Cu/Fe] versus metallicity ([Fe/H]) is almost solar for [Fe/H] > -1 and then decreases to a flat with [Cu/Fe] ~ -1.0 at [Fe/H] < -2.5.

While we can use several absorption lines to determine the copper abundances for stars with [Fe/H] > -1.0, this is not the situation for metal-poor stars with [Fe/H] < -1.5. For hot turnoff stars with effective temperatures from 6200 to 6500 K, the case is even worse. In such type stars, the Cu I is nearly fully ionized, leaving no neutral copper atoms in the excited levels. The only usable Cu abundance indicators are the two optical strongest Cu I lines at 5105 and 5782 Å in giant stars and the resonance lines at 3247 and 3273 Å in both dwarfs and giants. The advantage of the resonance lines is that they are very strong, and they remain measurable down to extremely low metallicities. Bihain et al. (2004) have been able to measure the 3273 Å line in the extremely metal-poor dwarf G64-12 ([Fe/H] ~ -3). Abundance derivations with these two strong lines are hindered mostly because they appear in a spectral range that is difficult to observe because of the lower flux in the UV for cool stars, and they are heavily blended by many other metal lines especially for metal-rich stars; a careful line synthesis needs to include all of the blend lines.

Copper abundances for cool stars were not investigated often; however, some local thermodynamic equilibrium (LTE) analysis, covering a large range of metal abundances, can be found from solar to metal-poor halo stars, such as the classical analysis of solar copper abundance by Kock & Richter (1968) and Simmerer et al. (2003). Based on six optical lines, Kock & Richter (1968) derived the solar Cu abundance of $\log \varepsilon_{\odot}({\rm Cu}) = 4.16 \pm 0.08$, while Simmerer et al. (2003) found that the λ5105 line gives an abundance in better agreement with the standard value: $\log \varepsilon_{\odot}({\rm Cu}) = 4.21$. Very recently, Bonifacio et al. (2010) performed three-dimensional line formation with hydrodynamical models for Cu lines in metal-poor stars, and they found that the Cu I resonance lines are not reliable abundance indicators. They suggested that the departure from LTE should be taken into account to properly describe these lines. And we have to rely on the resonance lines at 3247 and 3273 Å to derive the Cu abundances for very metal-poor stars. It should be noted that the ground state is over- or underpopulated due to atomic interaction processes, which will make systematic errors for an LTE abundance analysis. We will see below that the ground state of the $4s\,^2S$ level is depopulated due to the photoionization; thus, the non-local thermodynamic equilibrium (NLTE) effects for these two lines cannot be overlooked.

We describe the atomic model used in our analysis in Section 2. The two solar opacity sampling (OS) atmospheric models are shown in Section 3, and the NLTE calculation results obtained with different settings of the remaining free

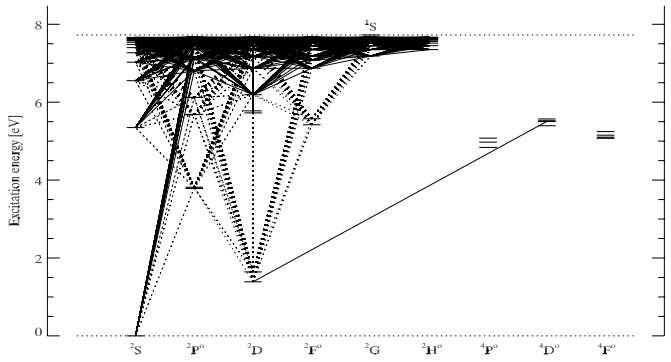

Figure 1. Grotrian diagram of Cu atomic model used in our analysis. Allowed transitions are the dotted lines, while the forbidden Cu I λ3010 line is continuous.

parameters are presented in Section 4. The photospheric solar Cu abundances determined with spectral line synthesis based on both LTE and NLTE assumption are discussed in Section 5, and the conclusions are presented in the last section.

2. METHOD OF CALCULATIONS

In this section, we briefly describe the copper model atom and the program used for calculating the copper level populations.

2.1. Atomic Model of Copper

The NIST database[5] and Sugar & Musgrove (1990) provide energy levels in neutral copper up to excitation energy $E \sim 7.558$ eV, in a total of 51 levels. The higher excitation energy levels and transition probabilities for the entire set of allowed transitions in Cu I and photoionization cross sections were calculated applying the *R*-matrix method described in detail by Liu et al. (2011). The *R*-matrix approach is a kind of close-coupling method to the analysis of electron–atom and photon–atom interactions, which was described in great detail by Burke et al. (1971). The scattering system consists of an atomic target with N electrons and an additional electron. The behavior of this system is determined solely by the electromagnetic interaction between the charged particles with all information on the system being contained in the wavefunction, which obeys the law of quantum mechanics. By solving the wavefunction of the system, one can obtain the required atomic data. The *R*-matrix method is one of the most accurate methods to obtain the atomic data such as energy levels, oscillator strengths, and photoionization cross sections. These atomic data are also the basic parameters to calculate the radiative opacity of astrophysical and laboratory plasmas (Zeng & Yuan 2002, 2006).

Our final atomic model is presented in Figure 1. It includes 96 levels of Cu I up to $n = 17$ ($L \leqslant 7$), roughly 0.06 eV below the ionization limit, and the ground state of Cu II ($3d^{10}\,^1S$). Fine structure was included for low-excitation levels to the $5p\,^2P^o$ term.

The atomic structure calculations provided radiative data for 1089 line transitions in Cu I. A simple Gauss profile was assumed with nine wavelength points each, when computing radiative rates for the bound–bound transitions.

We plot the photoionization cross sections calculated by Liu et al. (2014) and the corresponding hydrogenic approximations

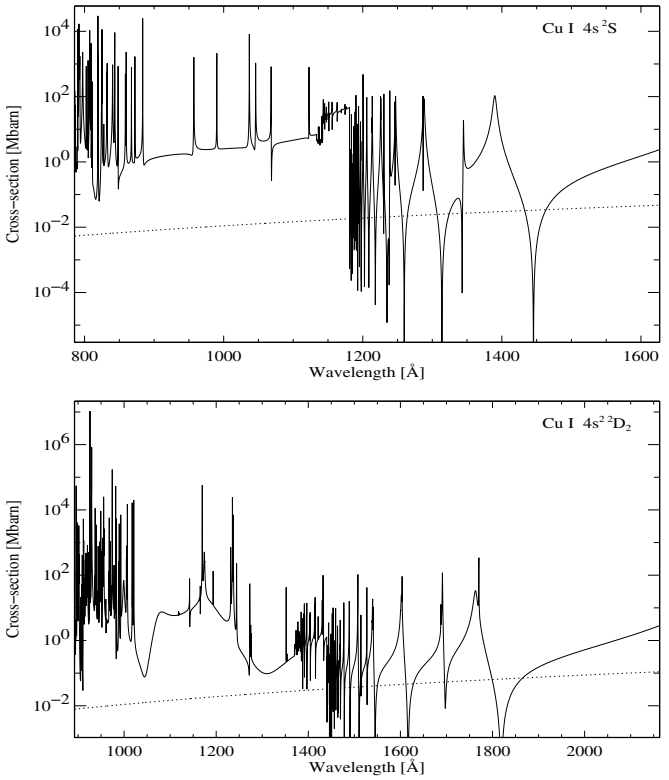

Figure 2. Photoionization cross sections for $4s\,^2S$ (top panel) and $4s^2\,^2D$ (bottom panel) levels as calculated by Liu et al. (2014). The corresponding hydrogenic approximations for the two cross sections (dotted curves) are significantly lower than the theoretical results.

for the lowest two terms, $4s\,^2S$ and $4s^2\,^2D$, in Figure 2; it is obvious that the results from hydrogenic approximations are significantly lower than those from the theoretical calculations. Also, we note that the calculated photoionization cross sections of the two lowest terms are about two orders of magnitude greater than those for other excited terms in the pertinent wavelength region of this work. A very similar situation was found for the levels in Mg I, Al I, and Si I (Baumüller & Gehren 1996; Zhao et al. 1998; Shi et al. 2008).

In our Cu NLTE computations both the *inelastic collisions* with electrons and hydrogen atoms for excitation and ionization are included. We use the formulae of van Regemorter (1962) and Allen (1973) to calculate the excitation of allowed and forbidden transitions by electron collisions, respectively, while the formula of Seaton (1962) is used to describe the ionization cross sections for electron collisions. The neutral hydrogen collisions are calculated based on the formula of Drawin (1968, 1969) described by Steenbock & Holweger (1984), and a similar formula is adopted for bound–free hydrogen collisions. It is noted that the Drawin formula significantly overestimates the collisional rates (Barklem et al. 2011); thus, a scaling factor S_H is used for some empirical correction to the Drawin approximations in our calculations.

2.2. Statistical Equilibrium Calculations

The method employed is similar to that described in Gehren et al. (2001). A revised DETAIL program (Butler & Giddings 1985) with accelerated lambda iteration has been used to solve the coupled radiative transfer and statistical equilibrium equations.

[5] http://www.physics.nist.gov/

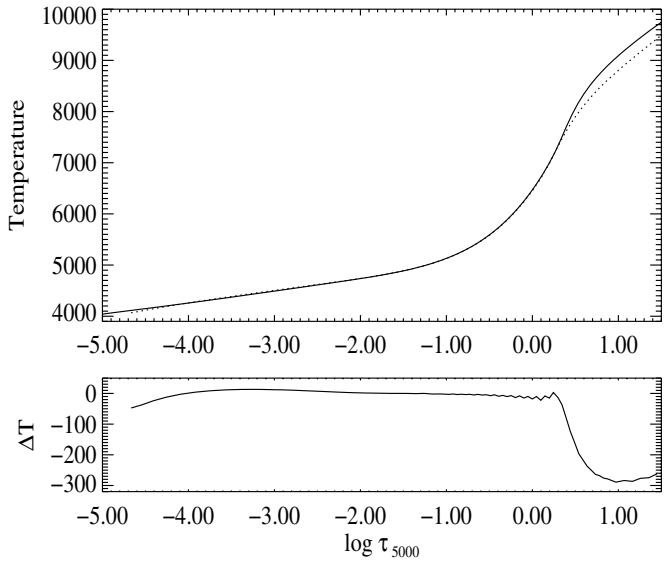

Figure 3. Comparison of the temperature structures of MAFAGS (solid) and MARCS (dotted line) OS solar models, and the temperature differences between these two solar models.

Background opacities. An OS code, which includes the hydrogen lines, the line lists from Kurucz (1994), and the important bound–free cross sections of hydrogen and the most abundant metals, is used to compute the background opacities. Zhao et al. (1998) have already pointed out that the background opacities are very important; the photoionization rates depend directly on them. Same as our previous works (Shi et al. 2008), *the background opacities are sampled on a random grid of between 5000 and 10,000 wavelengths, and the wavelengths of the line profiles are also added.* Around 14,000 wavelengths are sampled in the final NLTE line formation program. *Bound–bound* transition background opacities are sampled at the corresponding line frequencies (see Mashonkina et al. 2011, for details). All bound–bound transitions of Cu I were taken into account in the calculations, and the two strongest transitions were treated using Voigt profiles and the remaining transitions using depth-dependent Doppler profiles.

3. TWO OS SOLAR MODEL ATMOSPHERES

The basic background for the NLTE line formation and the spectrum synthesis depend on the solar atmosphere models. Our investigation is based on the standard one-dimensional model atmosphere in radiative-convective equilibrium. We apply the MAFAGS OS model, which is based on opacities sampled from continuous opacities and from an extended line list of Kurucz (2009) at 86,000 randomly chosen frequency points (Grupp 2004; Grupp et al. 2009), and the convection treated according to Canuto & Mazzitelli (1992). This model has been used in our previous NLTE computations (e.g., Mashonkina et al. 2011).

Since there exist other well-used OS models, e.g., MARCS model atmosphere (Gustafsson et al. 2008), it is interesting for us to extend our work to investigate the differences of the copper abundances between these two atmospheric models. Gustafsson et al. (2008) have discussed the physical assumptions, equations, and physical data of the MARCS OS model in detail, and Edvardsson (2008) has compared the broadband fluxes in the visible spectral region of F- and G-type MARCS model atmospheres to the spectrophotometric databases of the Sun and stars, and no systematic trend in the overall blue and red regions is found.

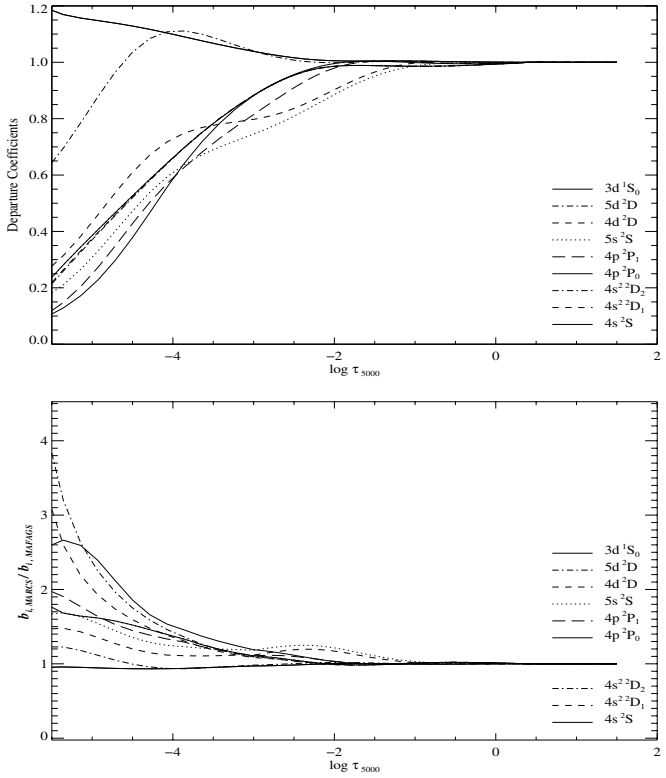

Figure 4. Departure coefficients $b_i = N_i^{\rm NLTE}/N_i^{\rm LTE}$ for selected Cu I levels and Cu II ground state as a function of the standard optical depth for our final Cu atomic model ($S_{\rm H} = 0.1$) calculated from an MAFAGS (top) OS solar model atmosphere. In the bottom, we compare the differences of the departure coefficients based on MARCS and MAFAGS OS models. Very similar results can be found for both atmospheric models.

We compare the temperature differences of MAFAGS and MARCS OS models in Figure 3. The differences are clearly inside $\log\tau = 0.3$; the ΔT goes up to 300 K. The gap between the temperature stratifications in the deepest layers is the result of different treatment of convection; MAFAGS models use the one of Canuto & Mazzitelli (1991), whereas MARCS models employ a standard mixing-length treatment (see Grupp 2004, for details). While outside $\log\tau \simeq -4.0$, the differences are about 40 K and show a slight increase with decreasing $\log\tau$, which may be due to the different sources of atomic data for bound–bound transitions adopted.

4. NLTE LINE FORMATION

We compare the departure coefficients of the lower Cu I levels and the Cu II ground state calculated for MAFAGS and MARCS OS solar models in Figure 4. We plotted the departure coefficients, $b_i = n_i^{\rm NLTE}/n_i^{\rm LTE}$, as a function of continuum optical depth $\tau_{\rm c}$, where, $n_i^{\rm NLTE}$ and $n_i^{\rm LTE}$ are the statistical equilibrium and Saha–Boltzmann (thermal) number densities, respectively (τ_{5000} referring to $\lambda = 5000$ Å). We present those levels necessary for subsequent line profile synthesis.

The departure coefficients $b_i = n_i^{\rm NLTE}/n_i^{\rm LTE}$ in the solar atmosphere presented in Figure 4 are best characterized by the underpopulation of the ground state $4s\,^2S$ and low-excitation levels $4s^2\,^2D$ far inside the atmosphere at optical depths around $\log\tau = 0.5$. This NLTE effect (overionization) is caused by superthermal radiation of non-local origin below the thresholds of

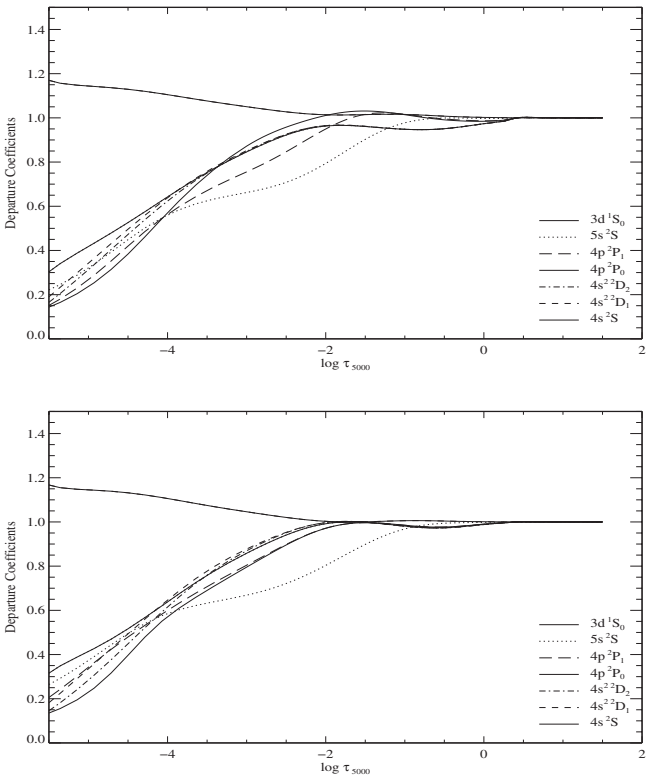

Figure 5. b_i ($N_i^{\rm NLTE}/N_i^{\rm LTE}$) as a function of log τ for our final Cu atomic model in the MAFAGS OS solar atmosphere. Same parameters as in Figure 4 are adopted, except that the electronic collision rates scaled by 0.1 (top), and the hydrogen collisions were ignored (bottom).

the $4s^2\,{}^2D$ levels. Photon loss in the strong line transitions starts around log $\tau_c = -2$, and this further depopulates the $4p\,{}^2P^{\rm o}$ and higher excitation levels. Another result is the overpopulation of the $5d\,{}^2D$ level outside log $\tau_c = -2$. The ground-state departure from LTE population is negligible around log $\tau_c = -2$, with the b_i again decreasing at smaller optical depths. Similar situations can be found for Al I and Si I (e.g., Baumüller & Gehren 1996; Shi et al. 2008, 2009).

In the bottom of Figure 4, we compare the differences of departure coefficients between the MARCS and MAFAGS OS solar models. Very similar results can be found in the region of log $\tau_c \leqslant -2$ for both models. However, the differences are larger in the upper atmosphere. Thus, it will not affect the bulk of line formation.

We have made test calculations using enhanced photoionization or reduced electronic collisions, and our results show that Cu I is not very sensitive to the atomic data. We note that the levels begin to depopulate already in deeper layers when the electron collision rates scaled by a factor of 0.1 (see Figure 5, top); however, the neutral Cu line formation is not affected much. The reason is that most of the visible and near-infrared solar lines are weak, and thus formed in deeper layers, while the two strong resonance lines at 3247 and 3273 Å remain thermalized to the upper photosphere.

The neutral hydrogen collision rates can be greatly stronger than the electron collision rates because of the large number of hydrogen atoms. In our calculations, we also investigate the influences due to the variation of hydrogen collision scaling factor $S_{\rm H}$ from 0 to 1. In the bottom of Figure 5, we show the departure coefficients when the hydrogen collision is ignored. Similar to the reduced electronic collision rates, the decrease of the hydrogen collision rates also results only in a minor dethermalization, which does not influence neutral copper line formation much. There are no significant variations in the line profiles when the $S_{\rm H}$ scales considered in this paper are changed; the abundance differences for $S_{\rm H} = 0$ and 1 cases are within 0.01–0.04 dex. Similar to Si and Fe (Shi et al. 2008; Mashonkina et al. 2011), we adopt $S_{\rm H} = 0.1$ for our final model.

The NLTE population computations were initially performed with a copper abundance of log $\varepsilon_\odot$(Cu) = 4.25. It was found that departures from LTE do not depend much on the exact value of the used copper abundance. The change of the copper abundance by 0.1 dex results in the variations in departure coefficients that, in turn, changed the derived abundance results by <0.005 dex.

5. LINE SYNTHESIS AND THE SOLAR Cu ABUNDANCE

In the analysis, 12 lines between 3100 Å < λ < 8100 Å were used, and we note that the resonance lines at 3247 and 3273 Å and the lines at 3010 and 5700 Å are heavily blended in the solar spectrum. We also note that there are some strong Cu II lines at the near-UV region; however, they are severely blended, and the analysis of these lines is beyond the scope of the present work. It is important for us to discuss gf values (the oscillator strengths) of these spectral lines before determining the solar copper abundance. In this paper, we adopted three sets of oscillator strengths and used them to compare the abundance differences: (1) the gf values were adopted from the experimental data of Kock & Richter (1968), which are very similar to those adopted by version 3.1.0 of the NIST Atomic Spectra Database (we also adopted the most recent gf values from Kono & Hattori (1982) for λ3010 and Carlsson (1988) for λ8092, as there are no experimental data from Kock & Richter 1968); (2) the values have been compiled by Bielski (1975); and (3) the calculated values from Liu et al. (2014). The hyperfine structure (HFS) components of the line transitions are computed based on the Russell–Saunders coupling method, and the magnetic dipole splitting constants, $A(J)$, and electric quadrupole splitting constants, $B(J)$, are taken from Biehl (1976). The isotopic fraction between ^{63}Cu and ^{65}Cu was assumed to be a fraction of 0.69 and 0.31, respectively (Asplund et al. 2009). We combine all components within 1 mÅ if the HFS components of the lines fall into more small intervals (see Table 1 for details). The synthetic NLTE profiles with and without HFS for the line of Cu I at 5700 Å in the solar flux spectrum are shown in Figure 6. We note that the van der Waals damping parameters are very important for Cu I strong lines in dwarf stars; thus, we calculate C_6 values from the Anstee & O'Mara (1991, 1995) tables. In Table 2, we present the parameters needed to determine the copper abundance for the selected lines, including the wavelengths, transitions, lower excitation energies, gf, and C_6 values.

We use the SIU program package from Reetz (1991) to perform the spectral line synthesis. This program is an IDL/Fortran-based software package. And the Kitt Peak Atlas (Kurucz et al. 1984) observed solar flux spectrum with resolution of ∼500,000 is adopted. All the line profiles were computed with various atomic parameters as drawn above. We adopted the solar model atmosphere with $T_{\rm eff} = 5777$ K, log $g = 4.44$, log $\varepsilon_\odot$(Cu) = 4.25, and a constant microturbulence velocity $\xi_t = 0.9\,{\rm km\,s^{-1}}$.

The synthetic spectra were convolved with a rotational velocity of 1.8 $\rm km\,s^{-1}$ and a radial-tangential macroturbulence Ξ_{rt} in order to fit the observed lines. It should be noted that

Table 1
Hyperfine Structure Components of Copper Lines

λ (Å)	E_{low}	j_{low}	j_{up}	log gf	log C_6
3010.826	1.38	2.5	2.5	−3.468	−31.268
3010.830	1.38	2.5	2.5	−3.482	−31.268
3010.833	1.38	2.5	2.5	−3.744	−31.268
3010.835	1.38	2.5	2.5	−2.925	−31.268
3010.837	1.38	2.5	2.5	−3.336	−31.268
3010.840	1.38	2.5	2.5	−3.073	−31.268
3010.844	1.38	2.5	2.5	−3.371	−31.268
3010.848	1.38	2.5	2.5	−3.044	−31.268
3010.850	1.38	2.5	2.5	−3.846	−31.268
3010.852	1.38	2.5	2.5	−3.491	−31.268
				−2.29	
3247.511	0.00	0.5	1.5	−1.383	−31.822
3247.513	0.00	0.5	1.5	−1.236	−31.822
3247.515	0.00	0.5	1.5	−1.033	−31.822
3247.517	0.00	0.5	1.5	−0.887	−31.822
3247.553	0.00	0.5	1.5	−0.935	−31.822
3247.554	0.00	0.5	1.5	−0.586	−31.822
3247.555	0.00	0.5	1.5	−1.383	−31.822
3247.556	0.00	0.5	1.5	−0.996	−31.822
3247.557	0.00	0.5	1.5	−1.732	−31.822
				−0.06	
3273.929	0.00	0.5	0.5	−1.405	−31.831
3273.932	0.00	0.5	0.5	−2.104	−31.831
3273.933	0.00	0.5	0.5	−1.078	−31.831
3273.936	0.00	0.5	0.5	−1.777	−31.831
3273.973	0.00	0.5	0.5	−1.405	−31.831
3273.974	0.00	0.5	0.5	−1.078	−31.831
3273.977	0.00	0.5	0.5	−1.405	−31.831
3273.978	0.00	0.5	0.5	−1.078	−31.831
				−0.35	
4022.625	3.79	0.5	1.5	−1.160	−30.403
4022.631	3.79	0.5	1.5	−0.939	−30.403
				−0.73	
4062.637	3.82	1.5	2.5	−1.704	−30.404
4062.638	3.82	1.5	2.5	−1.227	−30.404
4062.640	3.82	1.5	2.5	−1.006	−30.404
4062.644	3.82	1.5	2.5	−0.859	−30.404
				−0.50	
5105.487	1.39	2.5	1.5	−4.375	−31.902
5105.491	1.39	2.5	1.5	−3.421	−31.902
5105.493	1.39	2.5	1.5	−3.375	−31.902
5105.495	1.39	2.5	1.5	−4.551	−31.902
5105.500	1.39	2.5	1.5	−3.308	−31.902
5105.503	1.39	2.5	1.5	−3.053	−31.902
5105.509	1.39	2.5	1.5	−4.024	−31.902
5105.513	1.39	2.5	1.5	−3.070	−31.902
5105.515	1.39	2.5	1.5	−2.873	−31.902
5105.516	1.39	2.5	1.5	−4.201	−31.902
5105.520	1.39	2.5	1.5	−2.803	−31.902
5105.521	1.39	2.5	1.5	−2.958	−31.902
5105.524	1.39	2.5	1.5	−2.702	−31.902
5105.535	1.39	2.5	1.5	−3.055	−31.902
5105.540	1.39	2.5	1.5	−2.453	−31.902
5105.544	1.39	2.5	1.5	−2.597	−31.902
5105.562	1.39	2.5	1.5	−2.247	−31.902
				−1.51	
5153.232	3.77	0.5	1.5	−0.441	−30.971
5153.241	3.77	0.5	1.5	−0.219	−30.971
				−0.01	
5218.200	3.80	1.5	2.5	−0.934	−30.972

Table 1
(Continued)

λ (Å)	E_{low}	j_{low}	j_{up}	log gf	log C_6
5218.202	3.80	1.5	2.5	−0.457	−30.972
5218.206	3.80	1.5	2.5	−0.236	−30.972
5218.211	3.80	1.5	2.5	−0.089	−30.972
				+0.27	
5220.071	3.80	1.5	1.5	−1.816	−30.972
5220.073	3.80	1.5	1.5	−1.338	−30.972
5220.077	3.80	1.5	1.5	−1.117	−30.972
5220.082	3.80	1.5	1.5	−1.131	−30.972
5220.083	3.80	1.5	1.5	−1.481	−30.972
				−0.61	
5700.143	1.64	1.5	1.5	−4.056	−31.926
5700.159	1.64	1.5	1.5	−3.852	−31.926
5700.164	1.64	1.5	1.5	−4.454	−31.926
5700.166	1.64	1.5	1.5	−4.056	−31.926
5700.173	1.64	1.5	1.5	−3.706	−31.926
5700.188	1.64	1.5	1.5	−3.502	−31.926
5700.193	1.64	1.5	1.5	−4.104	−31.926
5700.194	1.64	1.5	1.5	−3.910	−31.926
5700.195	1.64	1.5	1.5	−3.706	−31.926
5700.200	1.64	1.5	1.5	−3.755	−31.926
5700.205	1.64	1.5	1.5	−3.852	−31.926
5700.221	1.64	1.5	1.5	−3.560	−31.926
5700.227	1.64	1.5	1.5	−3.405	−31.926
5700.231	1.64	1.5	1.5	−3.502	−31.926
5700.260	1.64	1.5	1.5	−3.308	−31.926
5700.266	1.64	1.5	1.5	−3.910	−31.926
5700.279	1.64	1.5	1.5	−2.956	−31.926
5700.285	1.64	1.5	1.5	−3.560	−31.926
				−2.34	
5782.034	1.64	1.5	0.5	−3.498	−31.938
5782.042	1.64	1.5	0.5	−3.799	−31.938
5782.054	1.64	1.5	0.5	−3.100	−31.938
5782.064	1.64	1.5	0.5	−3.150	−31.938
5782.073	1.64	1.5	0.5	−3.451	−31.938
5782.084	1.64	1.5	0.5	−2.752	−31.938
5782.085	1.64	1.5	0.5	−3.100	−31.938
5782.097	1.64	1.5	0.5	−3.100	−31.938
5782.113	1.64	1.5	0.5	−2.752	−31.938
5782.124	1.64	1.5	0.5	−2.752	−31.938
5782.153	1.64	1.5	0.5	−2.652	−31.938
5782.172	1.64	1.5	0.5	−2.304	−31.938
				−1.78	
8092.603	3.80	1.5	0.5	−2.179	−31.476
8092.604	3.80	1.5	0.5	−1.831	−31.476
8092.612	3.80	1.5	0.5	−0.971	−31.476
8092.625	3.80	1.5	0.5	−0.523	−31.476
8092.638	3.80	1.5	0.5	−1.530	−31.476
8092.639	3.80	1.5	0.5	−1.878	−31.476
8092.642	3.80	1.5	0.5	−1.132	−31.476
8092.644	3.80	1.5	0.5	−1.480	−31.476
8092.651	3.80	1.5	0.5	−1.132	−31.476
8092.653	3.80	1.5	0.5	−1.480	−31.476
				−0.16	

Notes. We adopted the log gf values from Kono & Hattori (1982), Kock & Richter (1968), and Carlsson (1988), while the van der Waals damping constants (log C_6) for Cu I lines are calculated according to the Anstee & O'Mara (1991, 1995) tables. The isotopic fraction between ^{63}Cu and ^{65}Cu was assumed to be a fraction of 0.69 and 0.31, respectively (Asplund et al. 2009). We combine all components within 1 mÅ if the HFS components of the lines fall into smaller intervals.

Table 2
Atomic Data of Copper Lines

λ (Å)	Transition	E_{low} (eV)	log gf			log C_6	log $\varepsilon_\odot$		log $\varepsilon_\odot$ (NLTE)		EW
					(LTE)	0.0	0.1	1.0			
3010.834	$4s^2\,^2D_{5/2}-4p\,^4D_{5/2}$	1.389	−1.975[a]	−2.29[b]	–	−30.86	4.10	4.12	4.11	4.10	23.4
3247.540	$4s\,^2S_{1/2}-4p\,^2P^o_{3/2}$	0.0	−0.062[a]	−0.06[c]	−0.06[f]	−31.73	4.09	4.13	4.11	4.09	285.9
3273.957	$4s\,^2S_{1/2}-4p\,^2P^o_{1/2}$	0.0	−0.359[a]	−0.35[c]	−0.36[f]	−31.74	4.11	4.13	4.12	4.11	239.4
4022.625	$4p\,^2P^o_{1/2}-5d\,^2D_{3/2}$	3.786	−0.855[a]	−0.73[c]	−0.62[f]	−29.60	4.24	4.27	4.25	4.25	11.9
4062.641	$4p\,^2P^o_{3/2}-5d\,^2D_{5/2}$	3.817	−0.506[a]	−0.50[c]	−0.36[f]	−29.60	4.20	4.22	4.21	4.20	16.7
5105.541	$4s^2\,^2D_{5/2}-4p\,^2P^o_{3/2}$	1.389	−1.516[a]	−1.51[c]	−1.66[f]	−31.67	4.10	4.13	4.12	4.10	89.9
5153.235	$4p\,^2P^o_{1/2}-4d\,^2D_{3/2}$	3.786	0.217[a]	−0.01[c]	0.06[f]	−30.57	4.35	4.36	4.35	4.35	46.3
5218.202	$4p\,^2P^o_{3/2}-4d\,^2D_{5/2}$	3.817	0.476[a]	0.27[c]	0.32[f]	−30.57	4.24	4.27	4.26	4.25	51.5
5220.070	$4p\,^2P^o_{3/2}-4d\,^2D_{3/2}$	3.817	−0.448[a]	−0.61[c]	−0.67[f]	−30.57	4.23	4.25	4.24	4.23	14.7
5700.240	$4s^2\,^2D_{3/2}-4p\,^2P^o_{3/2}$	1.642	−2.312[a]	−2.34[c]	−2.61[f]	−31.65	3.99	4.02	4.00	3.99	22.9
5782.132	$4s^2\,^2D_{3/2}-4p\,^2P^o_{1/2}$	1.642	−1.720[a]	−1.78[c]	−1.91[f]	−31.66	4.13	4.15	4.14	4.13	79.0
8092.634	$4p\,^2P^o_{3/2}-5s\,^2S_{1/2}$	3.817	−0.045[a]	−0.16[d]	−0.22[f]	−30.62	4.31	4.25	4.26	4.28	44.1
All 12 lines							4.17 ± 0.10	4.19 ± 0.09	4.18 ± 0.10	4.17 ± 0.10	
Without the two strong resonance lines							4.19 ± 0.11	4.20 ± 0.10	4.19 ± 0.10	4.19 ± 0.11	

Notes. The oscillator strength (log gf) values were adopted from the following references, and the van der Waals damping constants (log C_6) for Cu I lines are calculated based on the Anstee & O'Mara (1991, 1995) tables. Values for log $\varepsilon_\odot$ refer to MAFAGS OS atmosphere model and gf values of Kono & Hattori (1982); Kock & Richter (1968); Carlsson (1988).
[a] Bielski (1975).
[b] Kono & Hattori (1982).
[c] Kock & Richter (1968).
[d] Carlsson (1988).
[f] Liu et al. (2014).

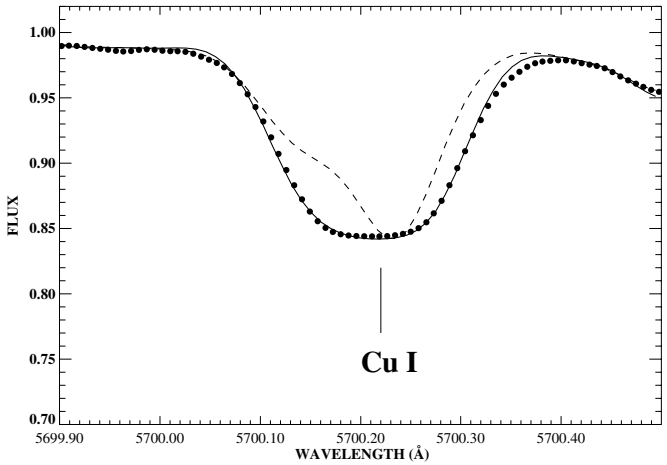

Figure 6. Synthetic NLTE profiles with (solid line) and without HFS (dashed line) for the line of Cu I at 5700 Å in the solar flux spectrum.

the radial–tangential macroturbulence Ξ_{rt} varies from 1.5 to 5.0 km s^{-1} depending on the different line formation depth. The comparison of NLTE synthetic profiles with the observed one is shown in Figure 7 for the selected copper lines.

Similar to Mg (Mashonkina 2013) and Si (Shi et al. 2008), we adopt $S_H = 0.1$ for our final atomic model. They are used to compute the statistical equilibrium and to derive solar Cu abundances below. The uncertainty of our abundance determination is less than 0.05 dex.

It is important to evaluate the consistency of the available gf values when determining the solar Cu abundance. In Figure 8, the gf values from Bielski (1975) produce a large abundance *scatter* with solar abundance of log $\varepsilon_\odot$(Cu) = 4.10 ± 0.14. On the other hand, the gf values obtained from well-stabilized arc emission measurements by Kock & Richter (1968) are the only high-quality experiment data, with log $\varepsilon_\odot$(Cu) = 4.18 ± 0.10; however, the copper abundances with this set of oscillator strengths display a clear trend, namely, that the six low-excitation lines, with excitation energy of the lower level ($E_{exc} \leqslant 1.64$ eV), give a 0.14 dex lower mean solar abundance compared to these from the six higher level ($E_{exc} > 3.7$ eV) lines (see Figure 8(b)). The use of the predicted gf values from Liu et al. (2014) removes this discrepancy. We note that the two strong resonance lines at the UV region are heavily blended (see Figure 7) and that these two lines are sensitive to the damping constant (C_6) values. Without these two strong resource lines, the solar mean NLTE abundance from 10 lines of Cu I is log $\varepsilon_\odot$(Cu) = 4.19 ± 0.10 when the gf values from Kock & Richter (1968) were adopted, while it is 4.24 ± 0.08 when the gf values from Liu et al. (2014) were adopted for the nine lines, which are perfectly consistent with the meteoritic value 4.25 ± 0.05 of Lodders et al. (2009).

It is interesting to investigate the influence of NLTE and of the choice of the model atmosphere on the solar abundances, which can be best viewed with the line wavelength as an x-axis. In Figure 9(a), we show the copper abundance differences between NLTE ($S_H = 0.1$) and LTE as a function of wavelength; both results depend on line profile fitting using the MAFAGS OS solar model. It is noted that the mean abundance difference is small; however, the NLTE effect is remarkable for the near-infrared line at 8092 Å, which comes from the transition of $4p\,^2P^o_{3/2}$ to $5s\,^2S_{1/2}$, and the underpopulation of the upper level ($5s\,^2S_{1/2}$) can be obviously seen in Figure 4. The abundance differences derived from the final NLTE models between the MAFAGS and the MARCS OS solar atmosphere are presented in Figure 9(b). Our results show that the differences are very small (⩽0.02 dex). The reason is that the visible lines are formed inside log $\tau_{5000} = -2$, where the temperatures for both models are nearly the same. Although the line formation region

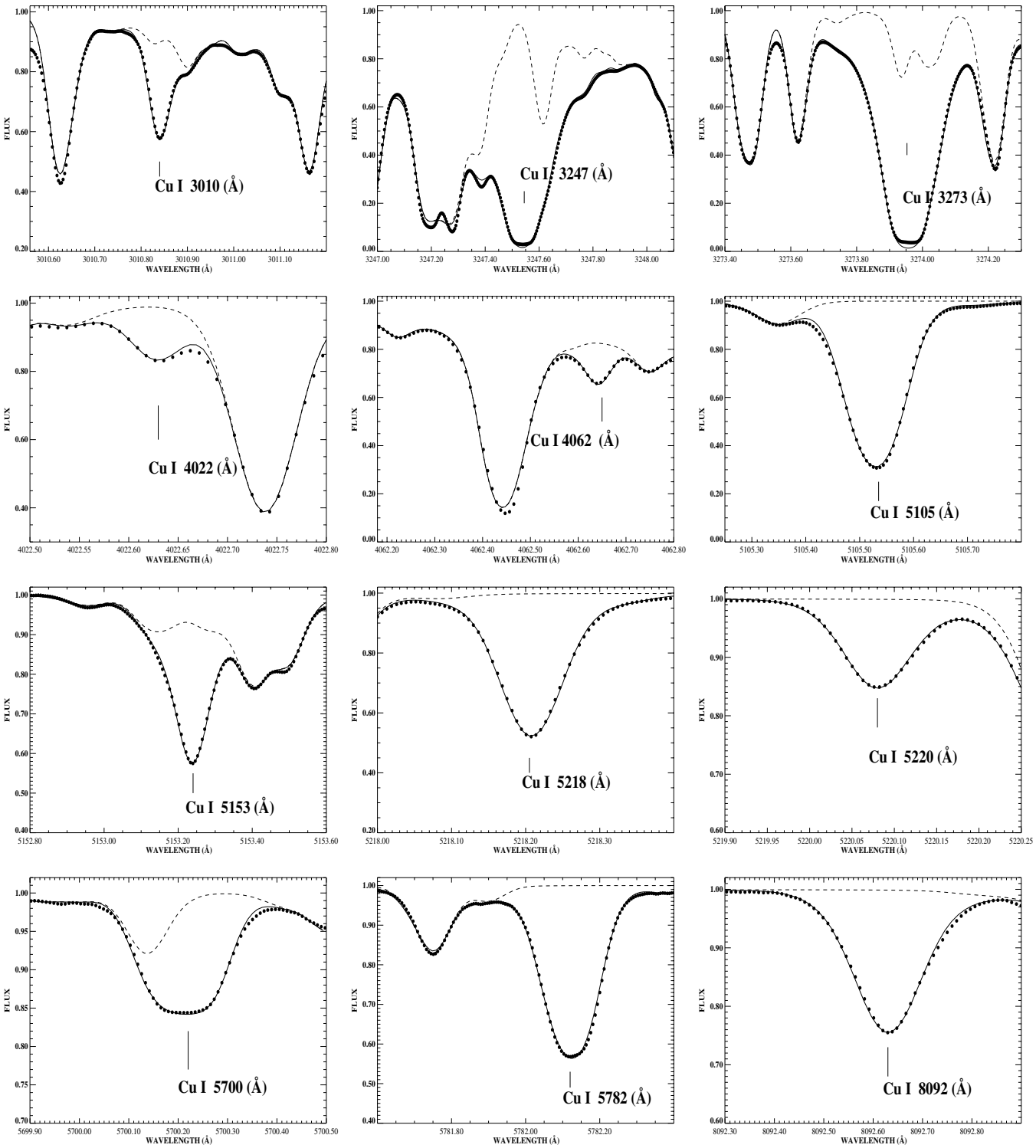

Figure 7. Best NLTE fits (continuous curves) of the solar lines of Cu I (filled circles). Everywhere, $S_{\rm H} = 0.1$. Dashed curves show the synthetic spectra computed without copper in the atmosphere.

of the two strongest UV lines is around $\log \tau_{5000} \sim -4.5$, the abundance determination is only slightly affected by the core of the strongest lines, which is dominated by the strong line wings forming in the region inside $\log \tau_{5000} = -2$. The differences between the normal electrical collision rates and these scaled by a factor of 0.1 for the MAFAGS OS model are shown in Figure 9(c). The differences are slightly larger for the lines from transitions of $4s^2\,^2D$ to $4p\,^2P^{\rm o}$; however, the mean Cu abundance is not very sensitive to the selection of the atomic models.

6. DISCUSSION

Based on the line profile fitting, the resulting copper abundances adopted the experimental gf values from Kock & Richter (1968) and Kono & Hattori (1982), and the theoretical values of Carlsson (1988) are shown in Table 2. In our investigation, the

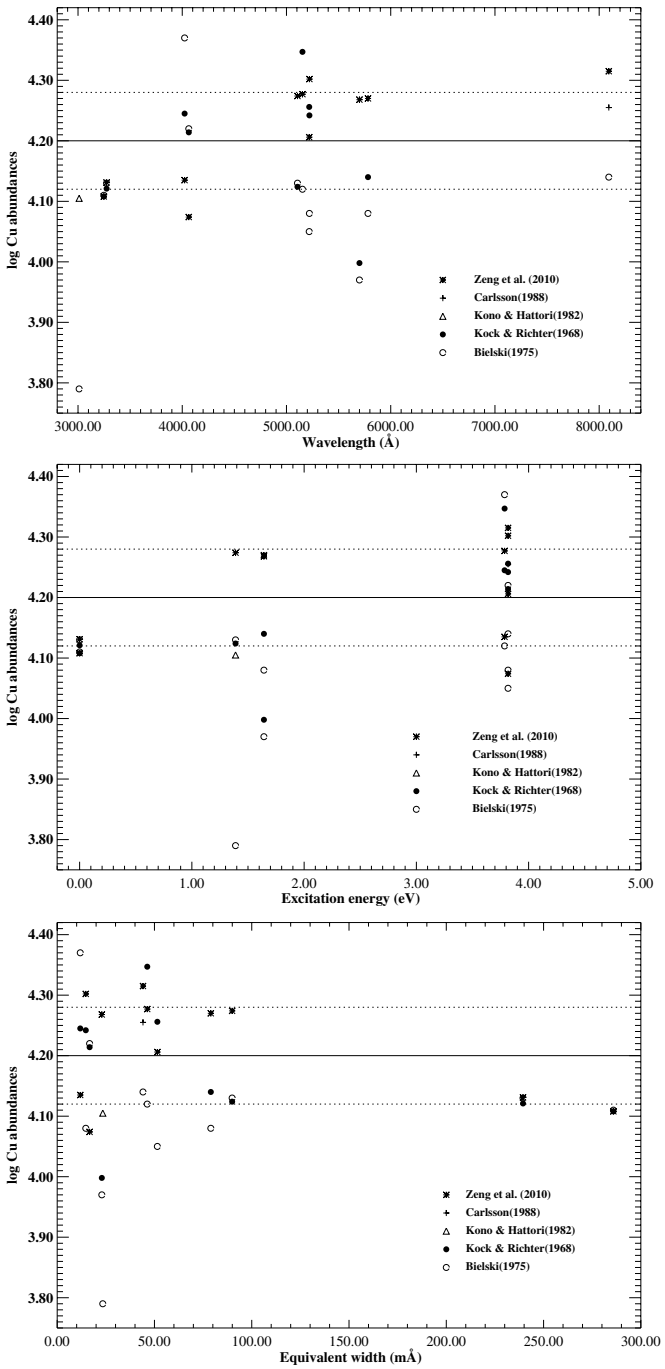

Figure 8. Solar copper abundances derived from three different sets of gf values. The straight line is the mean value only for the Kock & Richter (1968) data, while the dotted line represents the $\pm 1\sigma$ error.

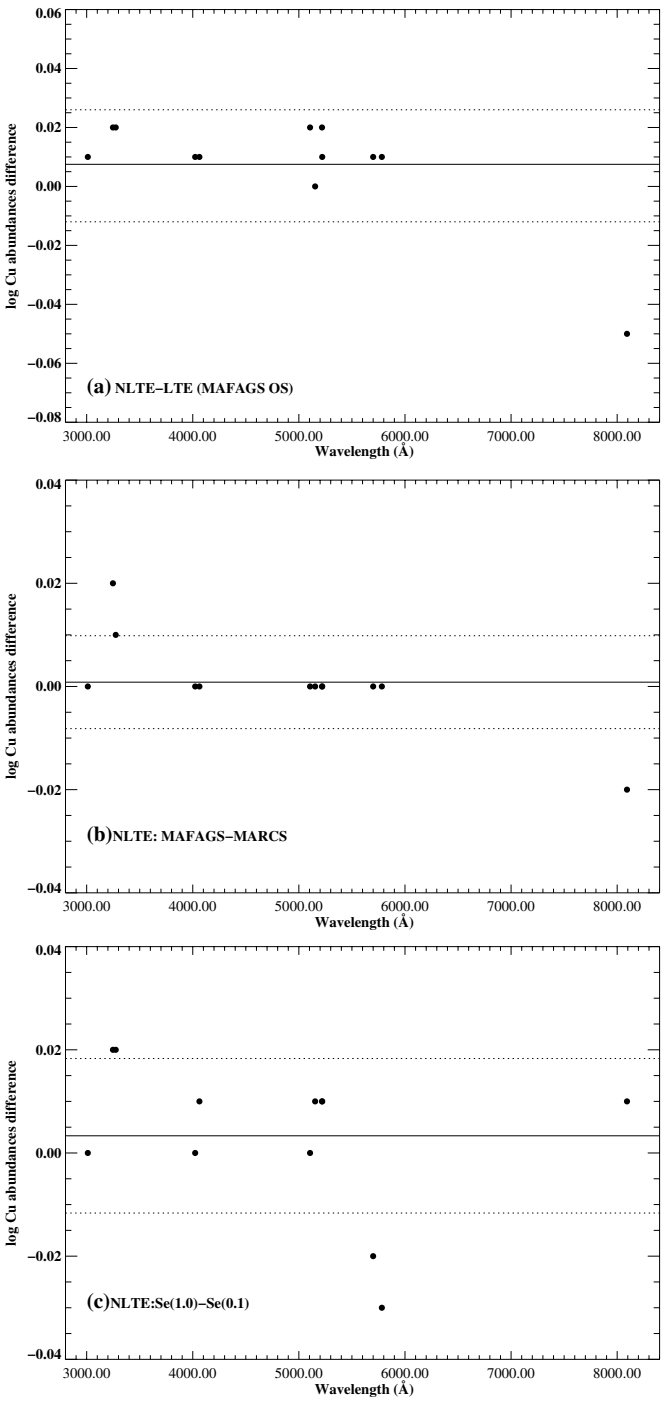

Figure 9. Solar copper abundance differences for all 12 lines.

solar lines from near-UV to the red visible are included, and our results show that the dispersion of the copper abundance results derived from different lines is small when the gf values from Liu et al. (2014) were adopted. The mean solar copper abundance of the nine lines excluding two strong resonance lines is $\log \varepsilon_{\odot}(\mathrm{Cu}) = 4.24 \pm 0.08$, which is in accordance with the value of 4.19 ± 0.04 determined by Grevesse et al. (2010), and in perfect accordance with the meteoritic abundance result of 4.25 ± 0.04 presented in Lodders et al. (2009).

It is noted that there may be a systematic abundance difference resulting from the solar model atmosphere (Gehren et al. 2001). In our investigation, the standard MAFAGS OS model atmosphere is adopted in the statistical equilibrium and the synthetic spectrum calculations. In Figure 3, we have shown that our MAFAGS OS model has higher temperatures around optical depth $\tau \simeq 0.3$ compared to the MARCS OS model; however, the temperature difference is only about 40 K or less around $\tau \simeq -4.0$, and thus the changes of the copper abundances can be negligible. Although there are three outlier points, the mean abundance difference between the MAFAGS and MARCS OS models is less than 0.004 dex. We have interpolated the MARCS OS model to have 80 depth points, which is the same as that of the MAFAGS model. Also the departure coefficients are very similar in the line-forming region ($\log \tau_c < -2$,

Figure 4(b)). Using the MAFAGS OS model atmosphere, the solar copper abundance based on the laboratory gf values of Kock & Richter (1968) is $\log \varepsilon_{\odot}(\mathrm{Cu}) = 4.19 \pm 0.10$, when the two strong resonance lines were ignored, which is 0.06 dex lower than the meteoritic copper abundance of 4.25. We note that the scatters in the single line abundances still exist (Figure 8), which may be due to the uncertain gf values for both calculated and experimental results. And it is easy to find from Table 2 that the differences are greater than 0.2 dex for some lines. Prochaska et al. (2000) have already found that there is considerable disagreement over the gf values.

Recently, it was found that the one-dimensional abundance analysis has systematic errors compared with three-dimensional results. Some of the solar metal abundances analyzed in three dimensions show slightly different results (Asplund et al. 2009). The recent analysis by Bonifacio et al. (2010) indicates that the LTE three-dimensional corrections of Cu I resonance lines for turnoff metal-poor stars are large, while they are small for giant stars. Thus, the solar abundance may need to consider the three-dimensional corrections (Asplund 2005).

This research was supported by the National Natural Science Foundation of China under grant Nos. 11021504, 11243004, 10973016, 11233004, and 10878024. L.M. thanks the Swiss National Science Foundation (SCOPES project No. IZ73Z0-128180/1) for partial support of this study.

REFERENCES

Allen, C. W. 1973, in Astrophysical Quantities (3rd ed.; London: Athlone Press)
Anstee, S. D., & O'Mara, B. J. 1991, MNRAS, 253, 549
Anstee, S. D., & O'Mara, B. J. 1995, MNRAS, 276, 859
Asplund, M. 2005, ARA&A, 43, 481
Asplund, M., Grevesse, N., Sauval, A. J., & Scott, P. 2009, ARA&A, 47, 481
Barklem, P. S., Belyaev, A. K., Spielfiedel, A., Guitou, M., & Feautrier, N. 2011, A&A, 530, A94
Baumüller, D., & Gehren, T. 1996, A&A, 307, 961
Biehl, D. 1976, Diplomarrbeit, Inst. f. Theor. Physik u. Sternwart, Kiel
Bielski, A. 1975, JQSRT, 15, 463
Bihain, G., Israelian, G., Rebolo, R., Bonifacio, P., & Molaro, P. 2004, A&A, 423, 777
Bonifacio, P., Caffau, E., & Ludwig, H.-G. 2010, A&A, 524, 96
Burke, P. G., Hibbert, A., & Robb, W. D. 1971, JPhB, 4, 153
Butler, K., & Giddings, 1985, J. Newsletter on the Analysis of Astronomical Spectra No. 9 (Univ. London)
Canuto, V. M., & Mazzitelli, I. 1991, ApJ, 370, 295
Canuto, V. M., & Mazzitelli, I. 1992, ApJ, 389, 724
Carlsson, J. 1988, PhRvA, 38, 1702
Cohen, J. G., Christlieb, N., McWilliam, A., et al. 2008, ApJ, 672, 320
Drawin, H. W. 1968, ZPhy, 211, 404
Drawin, H. W. 1969, ZPhy, 225, 483
Edwardsson, B. 2008, PhST, 133, 014011
Gehren, T., Butler, K., Mashonkina, L., Reetz, J., & Shi, J. R. 2001, A&A, 366, 981
Grevesse, N., Asplund, M., Sauval, A. J., & Scott, P. 2010, ApSS, 179, 183
Grupp, F. 2004, A&A, 420, 289
Grupp, F., Kurucz, R. L., & Tan, K. F. 2009, A&A, 503, 177
Gustafsson, B., Edvardsson, B., Jørgensen, U. G., Nordlund, Å, & Plez, B. 2008, A&A, 486, 951
Kock, M., & Richter, J. 1968, Z. Astrophys., 69, 180
Kono, A., & Hattori, S. 1982, JQSRT, 28, 383
Kurucz, R. L. 1994, SYNTHE Spectrum Synthesis Programs and Line Data, CD-ROM No. 18, Cambridge, MA
Kurucz, R. L. 2009, http://kurucz.harvard.edu/atoms/2600/, http://kurucz.harvard.edu/atoms/2601/, http://kurucz.harvard.edu/atoms/2602/
Kurucz, R. L., Furenlid, I., Brault, J., et al. 1984, in Solar Flux Atlas from 296 to 1300nm. Nat. Solar Obs. (New Mexico: Sunspot)
Liu, Y. P., Gao, C., Yuan, J. M., & Shi, J. R. 2014, ApJS, submitted
Liu, Y. P., Gao, C., Zeng, J. L., & Shi, J. R. 2011, A&A, 536, A51
Lodders, K., Palme, H., & Gail, H. P. 2009, in Landolt-Börnstein, New Series, Astronomy and Astrophysics, Vol. VI/4B, ed. J. E. Trumper, Chap. 4.4 (Berlin: Springer), 560
Mashonkina, L. 2013, A&A, 550, 28
Mashonkina, L., Gehren, T., Shi, J. R., Korn, A. J., & Grupp, F. 2011, A&A, 528, A87
Mishenina, T. V., Kovtyukh, V. V., Soubiran, C., Travaglio, C., & Busso, M. 2002, A&A, 396, 189
Pignatari, M., Gallino, R., Heil, M., et al. 2010, ApJ, 710, 1557
Prochaska, J. X., Naumov, S. O., Carney, B. W., et al. 2000, AJ, 120, 2513
Reetz, J. K. 1991, Diploma thesis, Universität München
Seaton, M. J. 1962, in Atomic and Molecular Processes, ed. D. R. Bates (New York: Academic Press)
Shi, J. R., Gehren, T., Butler, K., Mashonkina, L., & Zhao, G. 2008, A&A, 486, 303
Shi, J. R., Gehren, T., Mashonkina, L., & Zhao, G. 2009, A&A, 503, 533
Simmerer, J., Sneden, C., Ivans, I. I., et al. 2003, AJ, 125, 2018
Sneden, C., Gratton, R. G., & Crocker, D. A. 1991, A&A, 246, 354
Steenbock, W., & Holweger, H. 1984, A&A, 130, 319
Sugar, J., & Musgrove, A. 1990, JPCRD, 19, 527
van Regemorter, H. 1962, ApJ, 136, 906
Zeng, J. L., & Yuan, J. M. 2002, PhRvE, 66, 016401
Zeng, J. L., & Yuan, J. M. 2006, PhRvE, 74, 025401 (R)
Zhao, G., Butler, K., & Gehren, T. 1998, A&A, 333, 219